Superconducting states of the quasi-2D Holstein model: effects of vertex and non-local corrections

2005 J. Phys.: Condens. Matter 17 5663

(http://iopscience.iop.org/0953-8984/17/37/005)

INSTITUTE OF PHYSICS PUBLISHING JOURNAL OF PHYSICS: CONDENSED MATTER

J. Phys.: Condens. Matter **17** (2005) 5663–5676 doi:10.1088/0953-8984/17/37/005

Superconducting states of the quasi-2D Holstein model: effects of vertex and non-local corrections

J P Hague

Department of Physics and Astronomy, University of Leicester, Leicester LE1 7RH, UK

Received 22 April 2005, in final form 27 June 2005
Published 2 September 2005
Online at stacks.iop.org/JPhysCM/17/5663

Abstract

I investigate superconducting states in a quasi-2D Holstein model using the dynamical cluster approximation. The effects of spatial fluctuations (non-local corrections) are examined and approximations neglecting and incorporating lowest order vertex corrections are computed. The approximation is expected to be valid for electron–phonon couplings of less than the bandwidth. The phase diagram and superconducting order parameter are calculated. Effects which can only be attributed to theories beyond Migdal–Eliashberg theory are present. In particular, the order parameter shows momentum dependence on the Fermi surface with a modulated form and s-wave order is suppressed at half-filling. The results are discussed in relation to Hohenberg's theorem and the Bardeen–Cooper–Schrieffer approximation.

1. Introduction

The discovery of large couplings between electrons and the lattice in the cuprate superconductors has led to a call for more detailed theoretical studies of electron–phonon systems in low dimensions [1–3]. One of the best-known traditional approaches to the electron–phonon problem is attributed to Migdal and Eliashberg [4, 5]. In a bulk 3D system, the perturbation theory may be sharply truncated at first order and momentum dependence neglected if the phonon frequency is much less than the Fermi energy [4]. In physical terms, Migdal's approach requires that there is a very high probability that emitted phonons are reabsorbed in a last-in–first-out order. The typical materials of interest at the time were bulk metallic superconductors where electron–phonon coupling is relatively weak, and the phonon frequency small compared to the Fermi energy. For this reason, the application of Migdal–Eliashberg (ME) theory has been very successful and remains highly regarded.

Strong electron–phonon coupling and large phonon frequencies in low dimensional systems are outside the limits of validity of the Migdal–Eliashberg approach. Therefore, the aim of this paper is to evaluate and discuss the effects of both vertex corrections (VC) and spatial fluctuations on the theory of coupled electron–phonon systems in the superconducting state. This follows on from my work treating the normal (non-superconducting) state of the Holstein model using the dynamical cluster approximation (DCA) [6]. Initial attempts to include vertex

corrections were carried out by Engelsberg and Schrieffer [7]. Other previous attempts to extend ME theory include the introduction of vertex corrections into the Eliashberg equations by Grabowski and Sham [8], and an expansion to higher order in the Migdal parameter by Kostur and Mitrović to investigate the 2D electron–phonon problem [9]. Grimaldi *et al* generalized the Eliashberg equations to include momentum dependence and vertex corrections [10]. An anomalous hardening of the phonon mode was seen by Alexandrov and Schrieffer [11]. A discussion of the applicability of these and other approximations to the vertex function can be found in [12].

The current paper uses DCA to introduce a fully self-consistent momentum dependent self-energy. DCA extends DMFT by introducing short range fluctuations in a controlled manner [13]. It is particularly good at describing the electron–phonon problem, due to the limited momentum dependence of the self-energy and, in this case, the self-consistent DCA can be viewed as an expansion about the Eliashberg equations (in which momentum dependence is effectively coarse grained in a similar manner to in DMFT) [5]. In contrast to the Eliashberg equations, the full form of the Green's function is considered here, rather than the renormalized weak coupling Green's function (which has the form $\underline{G}^{-1}(\epsilon_k, \mathrm{i}\omega_n) = Z\mathrm{i}\omega_n\underline{\sigma}_0 - (\epsilon_k + \chi)\underline{\sigma}_3 - \Delta\underline{\sigma}_1$).

Two approximations for the electron and phonon self-energies are applied in this paper. The first neglects vertex corrections, but incorporates non-local fluctuations. The second incorporates lowest order vertex and non-local corrections. The vertex corrections allow the sequence of phonon absorption and emission to be reordered once, and therefore introduce exchange effects. The DCA result is compared to the corresponding DMFT result and in this way low dimensional effects are isolated. It should be noted that in the extreme strong coupling limit, the Holstein model forms a bipolaronic ground state, and perturbative methods in the electron and phonon Green's functions break down [14]. In the dilute limit, the Holstein model forms a polaronic liquid. There are significant differences between the weak and strong coupling limits of the polaron problem. In the strong coupling limit, the Lang–Firsov approximation may be applied, and physical properties have very different behaviour. For example the effective mass is reduced by an exponential factor of coupling. Exact numerical results show that the crossover between weak and strong coupling regimes occurs rapidly at $\lambda \sim 1$ [15]. For this reason, the present approximation should be considered valid for $|U| < W$.

The paper is organized as follows. In section 2, the DCA is introduced. In section 3, the Holstein model of electron–phonon interactions is described, and the perturbation theory and the full algorithm used in this work are detailed. In section 4, the results are presented. The momentum dependence of the superconducting order parameter is examined through the density of superconducting pairs. The phase diagram is then computed and comparison is made with analytical results. A summary of the major findings of this research is provided in section 5.

2. The dynamical cluster approximation

The dynamical cluster approximation [13, 16] is an extension to the dynamical mean-field theory. DMFT has been applied as an approximation to models of 3D materials [17–19]. However, application of DMFT to one- and two-dimensional models gives an incomplete description of the physics. An example of significant differences between two- and three-dimensional physics comes from quantum spin systems. In 3D, the Heisenberg model orders at a transition temperature, T_N. Significant non-local fluctuations in two dimensions reduce the Néel temperature to zero (Mermin–Wagner theorem), and the mean-field approach fails completely.

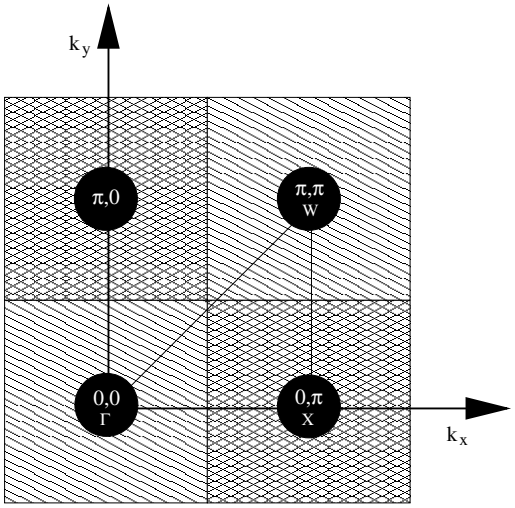

Figure 1. A schematic representation of the reciprocal-space coarse graining scheme for a four-site DCA. Within the shaded areas, the self-energy is assumed to be constant. There is a many-to-one mapping from the cross-hatched areas to the points at the centre of those areas. The coarse graining procedure corresponds to the mapping to a periodic cluster in real space, with spatial extent $N_c^{1/D}$. Also shown are the high symmetry points Γ, W and X, and lines connecting the high symmetry points. An infinite number of **k** states are involved in the coarse graining step, so the approximation is in the thermodynamic limit. DMFT corresponds to $N_C = 1$.

Conceptually, DCA is similar to DMFT. The Brillouin zone is divided up into N_C subzones consistent with the lattice symmetry (see figure 1). Within each of these zones, the self-energy is assumed to be momentum independent. For a system in the normal state, the Green's function is determined as

$$G(\mathbf{K}_i, z) = \int_{-\infty}^{\infty} \frac{\mathcal{D}_i(\epsilon)\,\mathrm{d}\epsilon}{z + \mu - \epsilon - \Sigma(\mathbf{K}_i, z)} \tag{1}$$

where $\mathcal{D}_i(\epsilon)$ is the non-interacting fermion density of states for subzone i, and the vectors $\mathbf{K}_i$ represent the average **k** for each subzone (plotted as the large dots in figure 1). The theory deals with the thermodynamic limit, and introduces non-local fluctuations with a characteristic length scale of $N_C^{1/D}$. For $N_C = 1$, DCA is equivalent to DMFT.

Since superconducting states are to be considered, DCA is extended within the Nambu formalism [20] in a similar manner to DMFT [17]. Green's functions and self-energies are described by 2×2 matrices, with off-diagonal anomalous terms relating to the superconducting states. Note that in the following equations 4-vectors are used, i.e. $\mathbf{K} \equiv (\mathrm{i}\omega_n, \mathbf{K})$. The Green's function and self-energy matrices have the components

$$\underline{G}(\mathbf{K}) = \begin{pmatrix} G(\mathbf{K}) & F(\mathbf{K}) \\ F^*(\mathbf{K}) & -G(-\mathbf{K}) \end{pmatrix} \tag{2}$$

$$\underline{\Sigma}(\mathbf{K}) = \begin{pmatrix} \Sigma(\mathbf{K}) & \phi(\mathbf{K}) \\ \phi^*(\mathbf{K}) & -\Sigma(-\mathbf{K}) \end{pmatrix}. \tag{3}$$

The coarse graining step is generalized to the superconducting state as

$$G(\mathbf{K}, \mathrm{i}\omega_n) = \int_{-\infty}^{\infty} \mathrm{d}\epsilon\, \frac{\mathcal{D}_i(\epsilon)(\zeta(\mathbf{K}_i, \mathrm{i}\omega_n) - \epsilon)}{|\zeta(\mathbf{K}_i, \mathrm{i}\omega_n) - \epsilon|^2 + \phi(\mathbf{K}_i, \mathrm{i}\omega_n)^2} \tag{4}$$

$$F(\mathbf{K}, \mathrm{i}\omega_n) = -\int_{-\infty}^{\infty} \mathrm{d}\epsilon \frac{\mathcal{D}_i(\epsilon)\phi(\mathbf{K}_i, \mathrm{i}\omega_n)}{|\zeta(\mathbf{K}_i, \mathrm{i}\omega_n) - \epsilon|^2 + \phi(\mathbf{K}_i, \mathrm{i}\omega_n)^2} \tag{5}$$

where $\zeta(\mathbf{K}_i, \mathrm{i}\omega_n) = \mathrm{i}\omega_n + \mu - \Sigma(\mathbf{K}_i, \mathrm{i}\omega_n)$.

The symmetry of the problem was constrained using the *pm*3*m planar* point group suitable for a 2D square lattice [21]. The partial DOS used in the self-consistent condition were calculated using the analytic tetrahedron method to ensure very high accuracy [22].

3. The Holstein model

A simple, yet non-trivial, model of electron–phonon interactions treats phonons as nuclei vibrating in a time-averaged harmonic potential (representing the interactions between all nuclei), i.e. only one frequency ω_0 is considered. The phonons couple to the local electron density via a momentum independent coupling constant g. The resulting *Holstein Hamiltonian* [23] is written as

$$H = -\sum_{\langle ij\rangle\sigma} t_{\langle ij\rangle\sigma} c^\dagger_{i\sigma} c_{j\sigma} + \sum_{i\sigma} n_{i\sigma}(g r_i - \mu) + \sum_i \left(\frac{M\omega_0^2 r_i^2}{2} + \frac{p_i^2}{2M} \right). \tag{6}$$

The first term in this Hamiltonian represents a tight binding model with hopping parameter t. Its Fourier transform takes the form $\epsilon_k = -2t\sum_{i=1}^{D}\cos(k_i)$. The second term connects the local ion displacement, r_i to the local electron density. Finally the last term can be identified as the bare phonon Hamiltonian, which is a simple harmonic oscillator. The creation and annihilation of electrons are represented by $c_i^\dagger$ and c_i respectively, p_i is the ion momentum and M the ion mass. $t = 0.25$ in this paper, corresponding to a bandwidth of $W = 2$. A small interplanar hopping of $t_\perp = 0.01$ is included to reduce the strength of the logarithmic singularity at $\epsilon = 0$ in $\mathcal{D}_{\pi,0}(\epsilon)$ and $\mathcal{D}_{0,\pi}(\epsilon)$ and stabilize the solution. This is only expected to modify the results at very low temperature for large clusters, and gives the problem a quasi-2D character.

It is possible to find an expression for the effective interaction between electrons by integrating out phonon degrees of freedom [24]. In Matsubara space, this interaction has the form

$$U(\mathrm{i}\omega_s) = \frac{U\omega_0^2}{\omega_s^2 + \omega_0^2}. \tag{7}$$

Here, $\omega_s = 2\pi s T$ represent the Matsubara frequencies for bosons and s is an integer. A variable $U = -g^2/M\omega_0^2$ is defined to represent the effective electron–electron coupling in the remainder of this paper.

When phonon frequency and coupling are small, Migdal's theorem applies. Migdal's approach allows vertex corrections to be neglected and becomes exact when $U \to 0^-$, $\omega_0 \to 0^+$ and is first order in U. In the limit of huge phonon frequency, the model maps onto an attractive Hubbard model, so the weak coupling limit of the Holstein model is only obtained by considering all second-order diagrams in U, and ME theory fails. The vertex-corrected theory described in this paper has the appropriate weak coupling behaviour for both large and small ω_0.

In this paper, perturbation theory to second order in U is used [19] (figure 2). The derivation of the perturbation theory in [19] made use of the conserving approximations of Bahm and Kadanoff [25, 24], which Miller *et al* then simplified by applying the dynamical mean-field theory (or local approximation). Here the theory has been extended to include partial momentum dependence through the application of the DCA. The electron self-energy has two terms: $\Sigma_{\mathrm{ME}}(\mathbf{K}, \mathrm{i}\omega_n)$ neglects vertex corrections (figure 2(a)) and $\Sigma_{\mathrm{VC}}(\mathbf{K}, \mathrm{i}\omega_n)$ corresponds

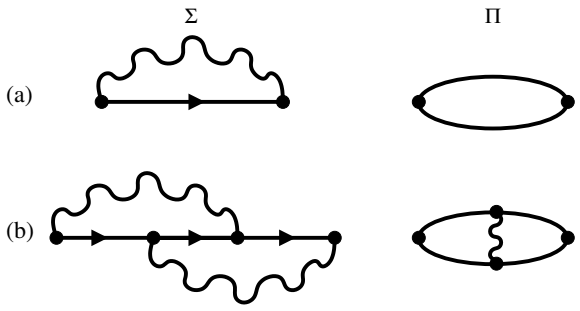

Figure 2. Diagrammatic representation of the approximation used in this paper. Series (a) represents the vertex-neglected theory which corresponds to the Migdal–Eliashberg approach. This is valid when there is a high probability that the last emitted phonon is the first to be reabsorbed, which is true if the phonon energy ω_0 and electron–phonon coupling U are small compared to the Fermi energy. Series (b) represents additional diagrams for the vertex-corrected theory. The inclusion of the lowest order vertex correction allows the order of absorption and emission of phonons to be swapped once. For moderate phonon frequency and electron–phonon coupling, these additions to the theory, in combination with non-local corrections, are expected to improve the theory to sufficient accuracy. The phonon self-energies are labelled with Π, and Σ denotes the electron self-energies. Lines represent the full electron Green's function and wavy lines the full phonon Green's function.

to the vertex-corrected case (figure 2(b)). $\Pi_{\mathrm{ME}}(\mathbf{K}, \mathrm{i}\omega_s)$ and $\Pi_{\mathrm{VC}}(\mathbf{K}, \mathrm{i}\omega_s)$ correspond to the equivalent phonon self-energies. The diagrams translate as follows:

$$\Sigma_{\mathrm{ME}}(\mathbf{K}) = UT \sum_{\mathbf{Q}} G(\mathbf{Q}) D(\mathbf{K}-\mathbf{Q}) \tag{8}$$

$$\phi_{\mathrm{ME}}(\mathbf{K}) = -UT \sum_{\mathbf{Q}} F(\mathbf{Q}) D(\mathbf{K}-\mathbf{Q}) \tag{9}$$

$$\Pi_{\mathrm{ME}}(\mathbf{K}) = -2UT \sum_{\mathbf{Q}} [G(\mathbf{Q})G(\mathbf{K}+\mathbf{Q}) - F(\mathbf{Q})F^*(\mathbf{K}+\mathbf{Q})] \tag{10}$$

$$\begin{aligned}\Sigma_{\mathrm{VC}}(\mathbf{K}) = (UT)^2 \sum_{\mathbf{Q}_1,\mathbf{Q}_2} & [G(\mathbf{Q}_1)G(\mathbf{Q}_2)G(\mathbf{K}-\mathbf{Q}_2-\mathbf{Q}_1) \\ & - F(\mathbf{Q}_1)G(\mathbf{Q}_2)F^*(\mathbf{K}-\mathbf{Q}_2-\mathbf{Q}_1) \\ & - F^*(\mathbf{Q}_1)G(\mathbf{Q}_2)F(\mathbf{K}-\mathbf{Q}_2-\mathbf{Q}_1) \\ & - G^*(\mathbf{Q}_1)F(\mathbf{Q}_2)F^*(\mathbf{K}-\mathbf{Q}_2-\mathbf{Q}_1)] \\ & \times D(\mathbf{K}-\mathbf{Q}_2)D(\mathbf{Q}_1-\mathbf{Q}_2)\end{aligned} \tag{11}$$

$$\begin{aligned}\phi_{\mathrm{VC}}(\mathbf{K}) = (UT)^2 \sum_{\mathbf{Q}_1,\mathbf{Q}_2} & [F^*(\mathbf{Q}_1)F(\mathbf{Q}_2)F(\mathbf{K}-\mathbf{Q}_2+\mathbf{Q}_1) \\ & - G(\mathbf{Q}_1)F(\mathbf{Q}_2)G(\mathbf{K}-\mathbf{Q}_2+\mathbf{Q}_1) \\ & - G^*(\mathbf{Q}_1)F(\mathbf{Q}_2)G^*(\mathbf{K}-\mathbf{Q}_2+\mathbf{Q}_1) \\ & - F(\mathbf{Q}_1)G(\mathbf{Q}_2)G^*(\mathbf{K}-\mathbf{Q}_2+\mathbf{Q}_1)] \\ & \times D(\mathbf{K}-\mathbf{Q}_2)D(\mathbf{Q}_1-\mathbf{Q}_2)\end{aligned} \tag{12}$$

$$\begin{aligned}\Pi_{\mathrm{VC}}(\mathbf{K}) = -(UT)^2 \sum_{\mathbf{Q}_1,\mathbf{Q}_2} & \mathrm{Tr}\left\{\underline{\sigma}_3\underline{G}(\mathbf{Q}_2+\mathbf{K})\underline{\sigma}_3\underline{G}(\mathbf{Q}_2)\underline{\sigma}_3\underline{G}(\mathbf{Q}_1)\underline{\sigma}_3\underline{G}(\mathbf{K}+\mathbf{Q}_1)\right\} \\ & \times D(\mathbf{Q}_2-\mathbf{Q}_1)\end{aligned} \tag{13}$$

where $\underline{\sigma}_3$ is the third Pauli matrix. $\underline{\Sigma} = \underline{\Sigma}_{\mathrm{ME}} + \underline{\Sigma}_{\mathrm{VC}}$ and $\Pi = \Pi_{\mathrm{ME}} + \Pi_{\mathrm{VC}}$.

The coarse grained phonon propagator $D(\mathbf{K}, \mathrm{i}\omega_s)$ is calculated from

$$D(\mathbf{K}, \mathrm{i}\omega_s) = \frac{\omega_0^2}{\omega_s^2 + \omega_0^2 - \Pi(\mathbf{K}, \mathrm{i}\omega_s)} \tag{14}$$

since the bare dispersion of the Holstein model is flat.

The time taken to perform the double integration over momentum and Matsubara frequencies is the main barrier to performing vertex-corrected calculations, and this limits the cluster size. Since the Holstein model with ω_0, $|U| \ll W$ (W is the bandwidth) has fluctuations which are almost momentum independent, the DCA has especially fast convergence in N_C for the parameter regime where ω_0, $|U| < W$, and calculations with relatively small cluster size accurately reflect the physics [6]. In this respect, finite size calculations take too long to compute, and the application of DCA to this problem is essential.

4. Results

In this section, I discuss results from the self-consistent scheme. Calculations are carried out along the Matsubara axis, with sufficient Matsubara points for an accurate calculation. The vertex-corrected self-energies drop off more quickly with the Matsubara frequency, so it is possible to increase efficiency by calculating for fewer frequencies. Typically, 256 Matsubara frequencies are used for the vertex-neglected diagrams, and 64 for the vertex-corrected diagrams, which reach asymptotic behaviour at smaller Matsubara frequencies. The scheme was iterated until the normal and anomalous self-energies had converged to an accuracy of approximately 1 part in 10^4. This corresponds to a very high accuracy for the Green's function.

Obtaining superconducting solutions involves an additional step, which is not obvious at the outset. Since the anomalous Green's function is proportional to the anomalous self-energy, initializing the problem with the non-interacting Green's function leads to a non-superconducting (normal) state. Also, the non-interacting Green's function is consistent with an ungapped state and opening a gap in the electron spectrum can lead to limit cycles during self-consistency, which are damped in the normal way [17].

To induce superconductivity, a constant superconducting field is applied to the whole system, leading to a non-zero anomalous Green's function, and automatically opening a gap in the normal-state Green's function. The procedure of applying a fictitious superconducting field is analogous to the application of a magnetic field to a spin system to induce a moment (the order parameter in that case). The superconducting field is applied by adding a constant term to the anomalous self-energy in equation (9). With the field applied, equations (4), (5) and (8)–(14) are solved self-consistently until convergence is reached. *Once satisfactory convergence is reached, the fictitious field is completely removed*. Iteration then continues until the true superconducting state is reached. This procedure corresponds to initializing the self-consistent cycle with a superconducting solution; note that similar techniques are used for obtaining Mott insulating solutions in the Hubbard model using DMFT [17].

By following this procedure, a superconducting state may be found below the transition temperature, T_C. Green's functions and self-energies computed in the superconducting state can then be used to initialize the self-consistent equations for similar couplings, fillings, temperatures (with an appropriate rescaling of the Matsubara frequencies) and phonon frequencies. Above the transition temperature, the magnitude of the anomalous Green's function tends to zero during iteration, as expected.

It is possible to see the generic effects of vertex and non-local corrections by examining the anomalous self-energy. In figure 3, the anomalous self-energy is shown for $n = 1.12$ and 1.54

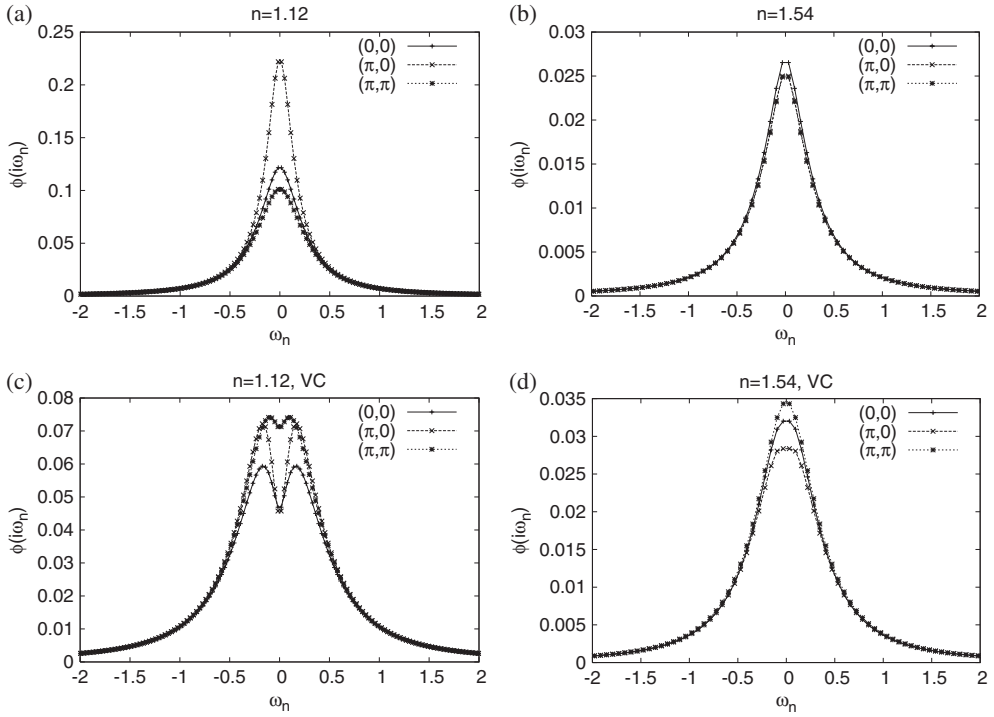

Figure 3. Real part of the anomalous self-energy at various fillings: (a) $n = 1.12$, no vertex corrections, (b) $n = 1.54$, no vertex corrections, (c) $n = 1.12$, vertex corrections, (d) $n = 1.54$, vertex corrections. Calculations were carried out at $T = 0.005$ with $|U| = 0.6$ and $\omega_0 = 0.4$. Momentum dependence corresponding to non-local corrections is clearly visible at half-filling, but drops off as the edge of the superconducting phase is reached. Vertex corrections are also most important at half-filling. There is a dip in the anomalous self-energy because the vertex corrections drop off more quickly in ω_n, with opposite sign to ϕ_{ME}, indicating that the approximation is close to breakdown at half-filling. The slight increase in the anomalous self-energy at $n = 1.54$ due to vertex corrections arises from a change in the form of the electronic Green's function. For half-filling, the Green's function at the van Hove points is pure imaginary, whereas for the dilute system, it is mostly real, so sums over products of Green's functions in the vertex can change sign.

for a cluster size of $N_{\mathrm{C}} = 4$ with parameters of $|U| = 0.6$, $T = 0.005$ and $\omega_0 = 0.4$ with and without vertex corrections. The panels are (a) $n = 1.12$, no vertex corrections, (b) $n = 1.54$, no vertex corrections, (c) $n = 1.12$, vertex corrections, (d) $n = 1.54$, vertex corrections. In panel (a), the momentum dependence of the vertex-neglected theory is clearly visible, and $\phi(\mathbf{K}, \mathrm{i}\omega_n)$ has a much larger value at the $(\pi, 0)$ point. Momentum dependence is significantly reduced as the system moves away from half-filling (panel (b)), indicating that Midgal–Eliashberg theory is more accurate in dilute systems. This is expected, since in very dilute systems, the electron density is sufficiently low that electrons meet very infrequently, and therefore the crossed diagrams of figure 2(b) make small contributions. By scanning vertically, the effect of including vertex corrections can be seen. Corrections are strongest close to half-filling, and drop off as the edge of the superconducting phase is reached. Migdal–Eliashberg theory is clearly quite accurate for dilute 2D systems, but it consistently fails close to half-filling. Initially, it seems as though vertex corrections are larger than the vertex-neglected results at $n = 1.12$. In fact, this is not the case. As discussed in [6], at half-filling, vertex corrections act to reduce the magnitude of the phonon self-energy, so there is much less renormalization

of the phonon propagator. A smaller phonon propagator means that the effective coupling is smaller, stabilizing the expansion in $\lambda_{\rm eff}$. There is a dip in the anomalous self-energy because the vertex corrections drop off more quickly in ω_n, with opposite sign to $\phi_{\rm ME}$, which is an indication that the approximation is close to breakdown at half-filling. The slight increase in the anomalous self-energy at $n = 1.54$ due to vertex corrections comes about from a change in form of the electronic Green's function. For half-filling, the Green's function at the van Hove points is pure imaginary, whereas for the dilute system, it is mostly real, so sums over products of Green's functions can change sign with respect to the Migdal–Eliashberg result. This sign change is also seen in DMFT simulations of the 3D Holstein model [19].

At this stage, it is appropriate to examine the size of the parameter $\lambda_{\rm eff}$ that defines the vertex correction expansion. Since the expansion in this case is in the full phonon Green's function, the expansion parameter is renormalized by the phonons, and reads $\lambda_{\rm eff} = |U\mathcal{D}(\mu)D(\mathrm{i}\omega_s = 0)|$, where $D(i\omega_s = 0)$ is the phonon propagator at zero Matsubara frequency. For dilute systems, $\mathcal{D}(\mu)$ is typically small, and so $\lambda_{\rm eff}$ is small (N.B. Unlike in 3D, $\mathcal{D}(\mu)$ is never zero in 2D, because of the discontinuity in the band edge of the non-interacting DOS). Close to half-filling, the DOS in 2D is divergent, and this parameter is expected to be large. In the current approximation, a small interplanar hopping was applied to stabilize the solution, so $\lambda_{\rm eff}$ is smaller than expected in a pure 2D system. As noted in [6], $D(0)$ is reduced by vertex corrections as compared to the Migdal–Eliashberg result. For most energies, the bare density of states in 2D is smaller than the bare density of states in 3D, since the divergence drops off logarithmically close to half-filling. Therefore, $\lambda_{\rm eff}$ is only really large for $n = 1$ within the current parameter range. For the intermediate to dilute limits, the relative magnitude of the second-order vertex correction goes like $\lambda^2 \sim 0.04$. At half-filling, with the current parameters, $\lambda^2 \sim 0.5$, so the approximation can only be considered to be qualitatively correct. Nonetheless, the current approximation has features appropriate to Hohenberg's theorem (discussed later) and the bare DOS drops off so quickly moving away from half-filling that results are expected to be accurate for most n.

How do the differences in the self-energy relate to observable quantities? One of the big questions in unconventional superconductivity concerns the possible forms that the order parameter can take, and a large discussion has grown up around issues such as the existence of unconventional order parameters such as extended s-wave and higher harmonics. To examine this idea, I demonstrate the evolution of the shape of the anomalous pairing density ($n_s(\mathbf{k}) = |T\sum_n F(\mathbf{k}, \mathrm{i}\omega_n)|$), which is related to the order parameter. In this paper, the superconducting order parameter is treated in a fully self-consistent manner within the lattice symmetry and no assumptions have been made in advance about its form.

Figure 4 shows the variation of superconducting pairing across the Brillouin zone. In all of the panels, $|U| = 0.6$, $\omega_0 = 0.4$, $n = 1$ and $T = 0.005$. A range of cluster sizes is shown. In the dynamical mean-field theory which corresponds to the Eliashberg solution (cluster size of $N_{\rm C} = 1$) the pairing is uniform around the Fermi surface, as is expected when momentum dependence is neglected. The inclusion of non-local momentum dependent fluctuations has a small, but significant, effect on the ordering. Pairing is reduced most at the $(\pi, 0)$ and $(0, \pi)$ points, leading to a visible peak at $(\pi/2, \pi/2)$. This demonstrates that the order parameter must necessarily include higher harmonics. For $N_{\rm C} = 64$ additional peaks are also seen. The additional features may be examined by determining the parameters of an expansion in spherical harmonics, $c_{lm} = \int \frac{\mathrm{d}^3\mathbf{k}}{(2\pi)^3} Y_{lm}(\theta, \phi) n_s(\mathbf{k})$ (figure 5). This shows that the anomalous density can be thought of as $m = 0$ harmonics with s, d, g, ... character, and additional harmonics with $m = \pm 4$ in the g channel. The harmonics can be quite large, especially away from half-filling, and undoubtedly need to be included if the superconductivity is to be described correctly.

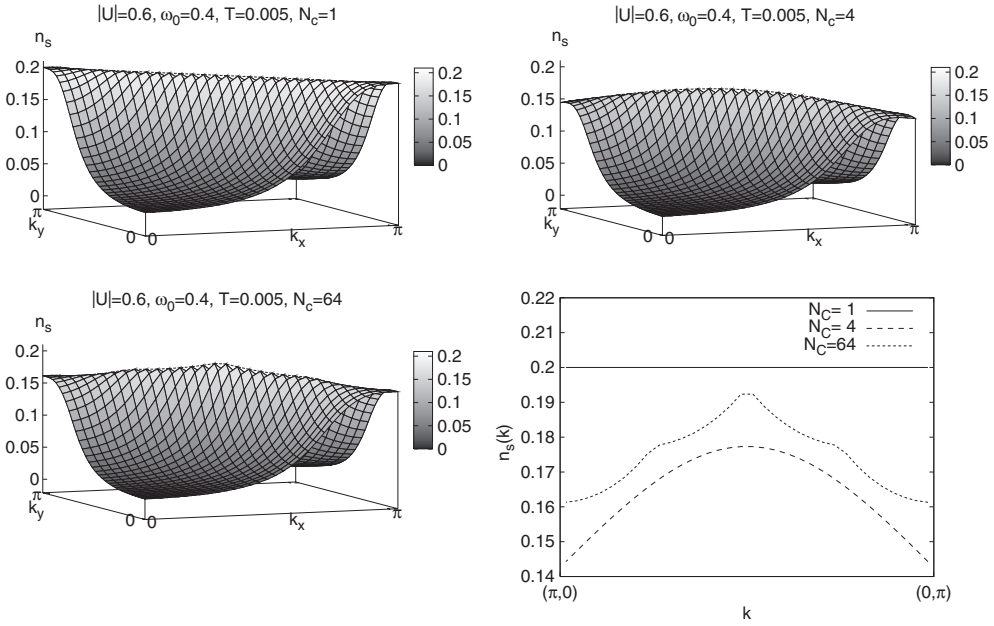

Figure 4. Variation of superconducting (anomalous) pairing density across the Brillouin zone. $|U| = 0.6, \omega_0 = 0.4, n = 1$ and $T = 0.005$. Cluster sizes are increased from $N_C = 1$ to 64. Pairing occurs between electrons close to the 'Fermi surface' at $\mathbf{k}$ and the opposite face of the surface at $-\mathbf{k}$. Also shown is the pairing density at the Fermi surface for the three different cluster sizes (bottom right). For a cluster size of $N_C = 1$ corresponding to DMFT, the pairing is uniform around the 'Fermi surface', demonstrating that momentum dependence has been neglected. Momentum dependence favours additional pairing along the $k_x = k_y$ line, and a peak can clearly be seen. The expansion in spherical harmonics contains even momentum states with $m = 0$. For $N_C = 64$, additional peaks can be seen, suggesting that the order parameter also contains extra higher order harmonics. The Fermi surface is not very clearly defined, with the mobile electrons spread out over a significant range of momentum states. $T = 0.005 \ll W$, so the spread should be very small in all locations in the Brillouin zone, except at the van Hove points, $(\pi, 0)$ and $(0, \pi)$, indicating that the spreading is due to the low dimensionality.

Figure 6 shows the variation of superconducting (anomalous) pairing density across the Brillouin zone as coupling and phonon frequency are changed. $T = 0.005, n = 1$ and $N_C = 4$ with vertex corrections excluded. As the phonon frequency is increased, the momentum dependence also increases. For $|U| = 0.9$, $\omega_0 = 0.05$, the order parameter is almost flat along the Fermi surface, indicating that DMFT is a good approximation for those parameters. Typically, additional coupling makes the order more uniform in the Brillouin zone. Note that for very strong coupling, the DMFT solution is expected to become exact, even in 2D, since the bare dispersion is then essentially flat, and the problem is completely local. For weak coupling and phonon frequency, there is a well defined Fermi surface. For the largest coupling and phonon frequencies (at the edge of applicability for the current approximation), the Fermi surface is practically destroyed.

It is of clear interest to map the phase diagram associated with superconducting order. First, the superconductivity arising from DMFT is investigated in the absence of vertex corrections. Figure 7 shows the resulting phase diagram. Note that in the DMFT solution, the superconductivity is strongest at half-filling and the order drops off monotonically as the filling increases. Assuming a form for the density of states in 2D (with small interplane hopping) of

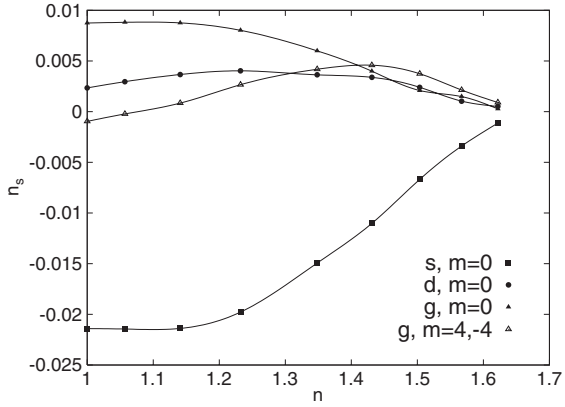

Figure 5. Harmonic decomposition of the anomalous density computed for $N_C = 64$ as the chemical potential is varied. It can be seen that pure s-wave states are the largest contributors to the anomalous density, followed by g and then d states with $m = 0$. Owing to the hump at the $(\pi/2, \pi/2)$ point, there are also g states with $m = \pm 4$. The $m = \pm 4$ states have equal magnitude, so $m_{\text{tot}} = 0$. Note that the relative contribution of higher harmonics is greatest away from half-filling.

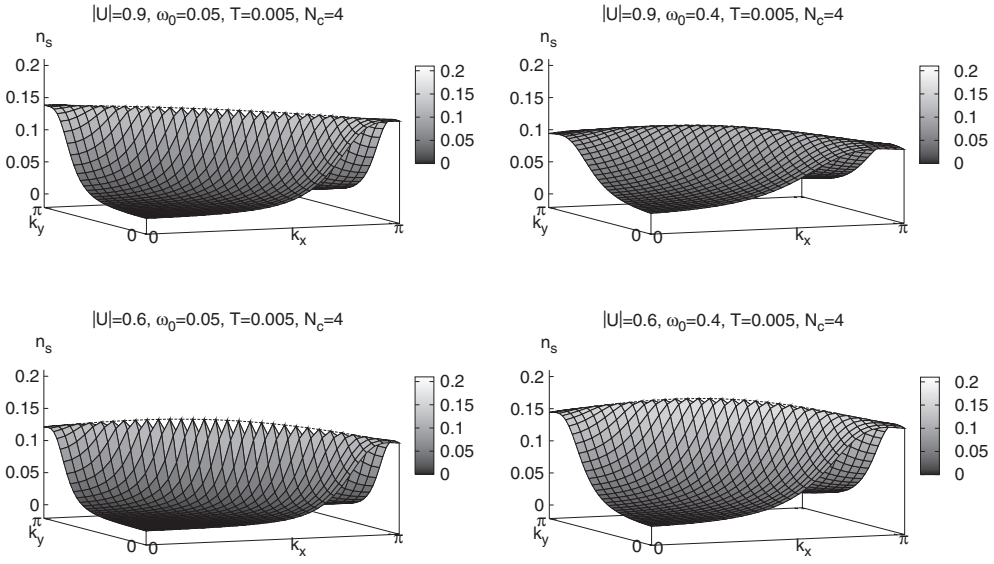

Figure 6. Variation of superconducting (anomalous) pairing density across the Brillouin zone. $T = 0.005$ and $N_C = 4$. Changes in the order parameter are shown as the coupling and phonon frequency are changed. As the phonon frequency is increased, the momentum dependence also increases, and the Fermi surface is less well defined. For $|U| = 0.9, \omega_0 = 0.05$, the order parameter is almost flat along the Fermi surface, indicating that DMFT is a good approximation for those parameters. For the largest coupling and phonon frequencies (at the edge of applicability for the current approximation), the Fermi surface is practically destroyed.

$\mathcal{D}(\epsilon) = (1 - t\log[(\epsilon^2 + t_\perp^2)/16t^2])/t\pi^2$ (for $|\epsilon| < 4t$) [26], the Bardeen–Cooper–Schrieffer (BCS) result may be calculated using the expression $T_C(n) = 2\omega_0 \exp(-1/|U|\mathcal{D}(\mu(n)))/\pi$, with the chemical potential taken from the self-consistent solution for a given n. This result also drops off monotonically. Results in the dilute limit are in good agreement with the BCS result.

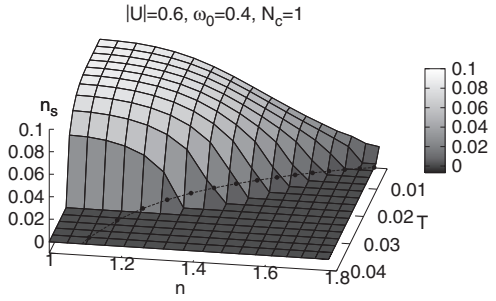

Figure 7. Superconducting phase diagram showing the total number of superconducting states. $|U| = 0.6, \omega_0 = 0.4$ and various T. A cluster size of $N_C = 1$ has been used, and no vertex corrections are included. The superconductivity is strongest at half-filling and the order drops off monotonically as the filling increases. Results in the dilute limit are in good agreement with the BCS result (the transition temperature from BCS is shown as the line with points in the $n_s = 0$ plane). Closer to half-filling, the DMFT result is significantly smaller than the BCS result (which predicts $T_C(n = 1) > 0.07$). The difference in results between the two mean-field theories at half-filling is due to the self-consistency in the DMFT.

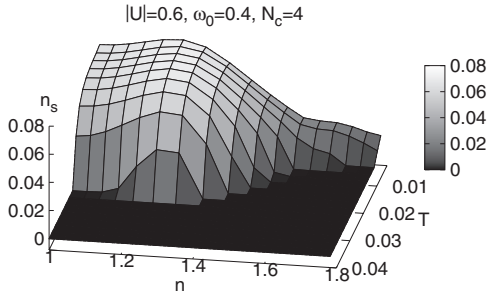

Figure 8. Superconducting phase diagram showing the total number of superconducting states. $|U| = 0.6, \omega_0 = 0.4$ and various T. A cluster size of $N_C = 4$ has been used, and no vertex corrections are included. There is an anomalous bump centred at about $n = 1.25$, indicating that the strongest superconductivity occurs away from half-filling. The highest transition temperature occurs for $T = 0.025$. The reduction in the transition temperature close to half-filling shows the onset of Hohenberg's theorem. The largest superconductivity coincides with the increase in components without pure s-wave character (see figure 5).

Closer to half-filling, the DMFT result is significantly smaller than the BCS result (which predicts $T_C(n = 1) > 0.07$). The difference in results between the two mean-field theories at half-filling is due to the self-consistency in the DMFT. For small U, the self-consistent equations essentially converge on the first iteration, but for larger U, the phonon and electron Green's functions are significantly renormalized, thus reducing the transition temperature.

To show the differences induced by spatial fluctuations, the phase diagram is computed for a cluster size of $N_C = 4$. Figure 8 shows the total density of superconducting pairs for $|U| = 0.6, \omega_0 = 0.4$ and various temperatures and fillings, without vertex corrections. Of most interest is an anomalous bump centred at about $n = 1.25$, indicating that the strongest superconductivity occurs away from half-filling, and that this is due to non-local fluctuations in 2D. Assuming a material with a non-interacting bandwidth of 1 eV, the highest transition temperature would correspond to 145 K. This value is higher than that eventually expected in real materials. For instance, the effect of a Coulomb pseudopotential U_C will be a reduction

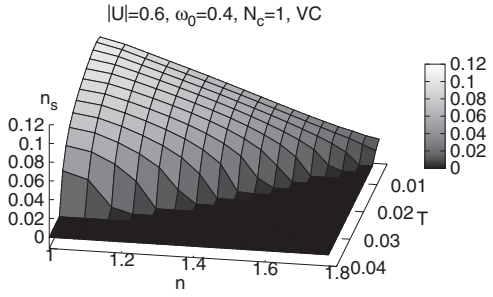

Figure 9. Superconducting phase diagram showing the total number of superconducting states. $|U| = 0.6$, $\omega_0 = 0.4$ and various T. A cluster size of $N_C = 1$ has been used, and vertex corrections are included. As in figure 7, the DMFT result falls off monotonically with increased filling.

of the transition temperature. The standard BCS result is modified by Coulomb repulsion in the following way: $T_C = 2\omega_0 \exp(-1/(\lambda - \mu_C))/\pi$, where $\mu_C = U_C \mathcal{D}(\mu)$.

In addition to the T_C reduction due to Coulomb repulsion, a fundamental limit on the transition temperature in pure 2D is set by Hohenberg theorem [27]. This is closely related to the effects of spatial fluctuations. The basis of Hohenberg's proof is the divergence of certain quantities (which are known to be finite) for $d \leqslant 2$ at $\mathbf{k} = 0$ when anomalous expectation values (e.g. the superconducting order parameter) are non-zero. In the DMFT solution, there are no specific $\mathbf{k} = 0$ states due to the coarse graining, and so the divergence in the correlation functions that led Hohenberg to determine that the order parameter must be zero for zero momentum pairing for $d \leqslant 2$ is washed out, leading to a finite transition temperature for the 2D local approximation. In DCA, partial momentum dependence is restored. Therefore, the effects of the washed out divergences are stronger. There is still a finite transition temperature, but it is reduced wherever there is strong momentum dependence. This is demonstrated by the drop in superconducting order at and close to half-filling in figure 8, where the momentum dependence is strongest. As the number of cluster points increases, the momentum resolution becomes superior, and the divergences of Hohenberg's theorem are expected to emerge in a systematic manner. In real materials with quasi-2D character, some interplane hopping remains. In that case, the results from small cluster DCA are expected to be more reliable.

Finally, I demonstrate the effects of vertex corrections on the superconducting phase diagram. Figures 9 and 10 show the total number of superconducting states as a function of filling and temperature for cluster sizes of $N_C = 1$ and 4 respectively. An electron–phonon coupling of $|U| = 0.6$ and phonon frequency of $\omega_0 = 0.4$ have been used. Vertex corrections do not appear to make a large difference to the DMFT result in figure 9. For $N_C = 4$, the bulge that was seen in the non-vertex-corrected phase diagram is very clearly enhanced. Superconductivity at half-filling is completely suppressed in the vertex-corrected solution. This is the precursor to Hohenberg's theorem applying across the entire phase diagram, and both the effects of spatial fluctuations and the lowest order vertex correction were essential to obtain that agreement.

5. Summary

In this paper I have carried out DCA calculations on a quasi-2D Holstein model in the superconducting state with large in-plane hopping and small out-of-plane hopping ($t = 0.25, t_\perp = 0.01$). Several approximations to the self-energy were considered, including

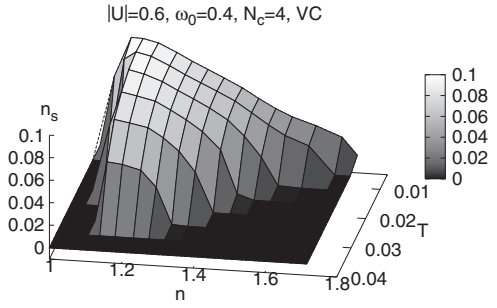

Figure 10. Superconducting phase diagram showing the total number of superconducting states. $|U| = 0.6$, $\omega_0 = 0.4$ and various T. A cluster size of $N_C = 4$ has been used, and vertex corrections are included. Superconducting states are suppressed at half-filling, and there is a significant bulge away from half-filling, with a maximum transition temperature of 0.015 W. It is significant that the transition temperature is reduced to zero at half-filling and suppressed close to half-filling, since reduction of transition temperatures is expected in 2D due to Hohenberg's theorem.

the neglect of vertex corrections (which corresponds to a momentum dependent extension to the Eliashberg theory), the inclusion of vertex corrections as a corrected approximation for stronger couplings and the introduction of spatial fluctuations. The anomalous self-energy, superconducting order parameter and phase diagram were calculated.

The superconducting order parameter was found to modulate around the Fermi surface, and is not a pure s-wave. Analysis of the harmonics showed that the state is a combination of s, d, f etc states with $m = 0$, and other states with integer value of $m = \pm 4n$. The total angular momentum is always zero. The contribution of the $m \neq 0$ states is considerably larger away from half-filling. Increases in bare phonon frequency tended to increase the strength of the superconducting order, and contributed to a degeneration of the Fermi surface.

The phase diagram was analysed for small cluster sizes of $N_C = 1, 4$. For $N_C = 1$, the phase diagram was shown to agree qualitatively with the BCS theory. When spatial fluctuations are included, the superconducting order is suppressed at half-filling, leading to a characteristic hump at a doping of approximately $\delta n = 0.25$. Vertex corrections completely suppress superconductivity at half-filling, which is believed to be a manifestation of Hohenberg's theorem. In particular, the states with the largest momentum dependence showed the strongest reduction in the transition temperature, indicating that spatial fluctuations as well as vertex corrections contribute to the suppression of superconducting order in pure 2D materials.

Acknowledgment

JPH would like to thank the University of Leicester for hospitality and use of facilities while carrying out this research.

References

[1] Lanzara A, Bogdanov P V, Zhou X J, Kellar S A, Feng D L, Lu E D, Yoshida T, Eisaki H, Fujimori A, Kishio K, Shimoyama J-I, Noda T, Uchida S, Hussa Z and Shen Z-X 2001 *Nature* **412** 6846
[2] McQueeny R J, Petrov Y, Egami T, Yethiraj M, Shirane G and Endoh Y 1999 *Phys. Rev. Lett.* **82** 628
[3] Zhao G M, Hunt M B, Keller H and Müller K A 1997 *Nature* **385** 236
[4] Migdal A B 1958 *JETP Lett.* **7** 996

[5] Eliashberg G M 1960 Interactions between electrons and lattice vibrations in a superconductor *JETP Lett.* **11** 696
[6] Hague J P 2003 Electron and phonon dispersions of the two dimensional Holstein model: effects of vertex and non-local corrections *J. Phys.: Condens. Matter* **15** 2535
[7] Engelsberg S and Schrieffer J R 1963 *Phys. Rev.* **131** 993
[8] Grabowski M and Sham L J 1984 Superconductivity from nonphonon interactions *Phys. Rev.* B **29** 6132
[9] Kostur V N and Mitrović B 1993 Electron–phonon interaction in two dimensions: variation of Im $\Sigma(\epsilon_p, \omega)$ with increasing ω_D/E_F *Phys. Rev.* B **48** 16388
[10] Grimaldi C, Pietrono L and Strässler S 1995 Nonadiabatic superconductivity: electron–phonon interaction beyond Migdal's theorem *Phys. Rev. Lett.* **75** 1158
[11] Alexandrov A S and Schrieffer J R 1997 *Phys. Rev.* B **56** 13731
[12] Danylenko O V and Dolgov O V 2001 Nonadiabatic contribution to the quasiparticle self-energy in systems with strong electron–phonon interaction *Phys. Rev.* B **63** 094506
[13] Hettler M, Tahvildar-Zadeh A N, Jarrell M, Pruschke T and Krishnamurthy H R 1998 Nonlocal dynamical correlations of strongly interacting electron systems *Phys. Rev.* B **58** 7475
[14] Alexandrov A S and Mott N F 1994 *Rep. Prog. Phys.* **57** 1197
[15] Kornilovitch P E 1998 *Phys. Rev. Lett.* **81** 5382
[16] Hettler M, Mukherjee M, Jarrell M and Krishnamurthy H R 2000 *Phys. Rev.* B **61** 12739
[17] Georges A, Kotliar G, Krauth W and Rozenburg M 1996 *Rev. Mod. Phys.* **68** 13
[18] Tahvildar-Zadeh A N, Freericks J K and Jarrell M 1997 Magnetic phase diagram of the Hubbard model in three dimensions: the second-order local approximation *Phys. Rev.* B **55** 942
[19] Miller P, Freericks J K and Nicol E J 1998 Possible experimentally observable effects of vertex corrections in superconductors *Phys. Rev.* B **58** 14498
[20] Maier T, Jarrell M, Pruschke T and Hettler M H 2004 Quantum cluster theories *Preprint* cond-mat/0404055
[21] Hahn T (ed) 1996 *International Tables for Crystallography* vol A *Space Group Symmetry* (Dordrecht: Kluwer–Academic)
[22] Lambin Ph and Vigneron J P 1984 Computation of crystal green's functions in the complex-energy plane with the use of the analytical tetrahedron method *Phys. Rev.* B **29** 3430
[23] Holstein T 1959 *Ann. Phys.* **8** 325
[24] Bickers N E and Scalapino D J 1989 *Ann. Phys.* **193** 206
[25] Bahm G and Kadanoff L P 1961 *Phys. Rev.* **124** 287
[26] Macarie L S and d'Ambrumenil N 1995 *J. Phys.: Condens. Matter* **7** 3237
[27] Hohenberg P C 1967 *Phys. Rev.* **158** 383